FOSSEE, IIT Bombay
OpenFOAM Case Study Project
June 2024

Fluid Solid Interaction (FSI) using solids4Foam

Lucky Babu Jayswal[1] and Chandan Bose[2]

[1]Undergraduate Student, Aerospace Engineering, IOE, Pulchowk Campus, Tribhuvan University
[2]Assistant Professor, Aerospace Engineering, College of Engineering and Physical Sciences, The University of Birmingham

June 25, 2024

Synopsis

Abstract

The objective of this case study project is to delve into the complexities and methodologies involved in solving Fluid-Solid Interaction (FSI) problems using the OpenFOAM toolbox, specifically solids4Foam. The study underscores the growing interest in FSI within the computational fluid dynamics (CFD) community due to its broad applicability across various engineering fields such as aerospace and mechanical engineering. This project emphasize the inherent challenges in FSI problems, primarily due to the dynamic mesh treatment required to accurately capture the interactions between fluids and solids. The core of the report is centered around the implementation and validation of the solids4Foam solver through two distinct case studies: the Hron-Turek benchmark and a Perpendicular Flap Case. The Hron-Turek case is a well-known benchmark in the FSI domain, used to evaluate the performance of different numerical methods and solvers. The Perpendicular Flap case involves a flexible flap interacting with a laminar incompressible flow within a rectangular channel, with the fluid inlet velocity varying parabolically. Both cases serve to validate the solver's accuracy by comparing the results against existing numerical data. Solids4Foam employs a partitioned approach to solve FSI problems, where the fluid and solid regions are solved separately, and a coupling algorithm enforces momentum and kinematic continuity at the interface. The report details the use of the Dirichlet-Neumann coupling algorithm, where the fluid domain is solved with a Dirichlet condition for velocity at the interface, and the solid domain is solved with a Neumann condition for traction. This method is crucial for ensuring stable and accurate solutions in FSI simulations.The report showcases the potential of solids4Foam as a powerful tool for solving FSI problems within the OpenFOAM framework. By addressing the key challenges and providing validated case studies, valuable insights into the capabilities and applications of this open-source solver are gained, reinforcing its utility for researchers and engineers in the field of computational mechanics.

Keywords: FSI, OpenFoam, CFD, solids4foam, HronTurek, Dirichlet, Neumann

1 Introduction

1.1 Theory

Solids4foam [1] is an OpenFOAM toolbox for computational solid dynamics and fluid-solid interactions (FSI). Currently, only the partitioned approach is implemented in soldis4foam. In the partitioned approach, the fluid and solid regions are solved separately and a coupling algorithm is used to enforce momentum and kinematic continuity at the fluid-solid interface. One such coupling algorithm is the Dirichlet-Neumann approach; this is currently implemented in solids4foam. In this approach, the fluid domain is solved with a Dirichlet condition for velocity at the interface, and the solid domain is solved with a Neumann condition (traction) at the interface as mentioned in [2].

The paper [3] describes a self-contained parallel fluid-structure interaction solver based on a finite volume discretisation, where a strongly coupled partitioned solution procedure is employed.The incompressible fluid flow is described by the Navier-Stokes equations in the arbitrary Lagrangian-Eulerian form, and the solid deformation is described by the Saint Venant Kirchhoff hyperelastic model in the total Lagrangian form. Both the fluid and the solid are discretised in space using the second-order accurate cell-centred finite volume method, and temporal discretisation is performed using the second-order accurate implicit scheme. The method, implemented in open-source software OpenFOAM, is parallelised using the domain decomposition approach and the exchange of information at the fluid-solid interface is handled using global face zones. The performance of the solver is evaluated in standard two- and threedimensional cases and excellent agreement with the available numerical results is obtained.

Fluid-Structure Interaction (FSI) benchmarks are crucial for evaluating numerical methods in computational mechanics, integrating fluid dynamics with structural mechanics to simulate interactions between fluid flow and structural deformations. Building on foundational benchmarks, such as Turek and Schäfer's laminar flow around a cylinder and Wall and Ramm's stabilized Arbitrary Lagrangian-Eulerian finite element method, this paper [4] proposes new benchmarks focusing on incompressible channel flow around an elastic object. The benchmarks emphasize capturing self-induced oscillations in the structure, a phenomenon sensitive to numerical accuracy and stability. Numerical methods for FSI are classified into partitioned and monolithic approaches, with significant contributions from Hron and Turek in developing monolithic solvers. The proposed benchmarks include detailed specifications of fluid and structural properties, boundary conditions, and domain geometry, using the Navier-Stokes equations for the fluid and linear elasticity for the structure. Key quantities for comparison are the y-coordinate of the beam's end over time and the fluid forces on the submerged body, providing a basis for assessing the performance of FSI solvers. Testing with different material properties, such as polybutadiene and polypropylene paired with glycerine, enhances the benchmarks' robustness.

The remaining report consists of two major parts for each case and each of them are divided into three major sections. Governing Equations and Models section, defines the problem, establishes the necessary governing equations, provides an overview of the geometry and the mesh, and details of the solver setup. Next section goes over the results. This section interprets the results of the grid convergence studies and validation of the results. The final section provides a conclusion of the study.

CASE 1: PerpendicularFlap

2 Governing Equations and Models

2.1 Problem definition

This study investigates the FSI between flexible flap and laminar incompressible flow. The geometry of the problem consists of a rectangular horizontal channel and a perpendicular flexible flap. The flap is attached at the bottom of the channel. The inlet velocity of the fluid varies parabolically with the width of the channel. Low Reynold's number flow of 25 is used in this case. Two different coupling algorithms are used for fluid-solid coupling and results obtained from them are compared with each other.

2.2 Governing equations

Fluid, solid, and the interface between them are governed by three sets of equations.

2.2.1 Fluid

We assume incompressible Newtonian isothermal laminar flow, where the Navier-Stokes governing equations take the form:

$$\boldsymbol{\nabla \cdot V} \;=\; 0 \tag{1}$$

$$\frac{\boldsymbol{\partial \mathbf{V}}}{\boldsymbol{\partial \mathbf{t}}} \;+\; \boldsymbol{V(\nabla \cdot V)} \;=\; \boldsymbol{\nu\, \nabla^2\, V} \;-\; \frac{1}{\rho}\boldsymbol{\nabla} p \;+\; f_b \tag{2}$$

where,
Bold symbol represents vector.
v = velocity vector
ν = Kinematic viscosity
f_b = force vector
p = pressure
ρ = density

2.2.2 Solid

We assume finite strains with the material behavior described by the neo-Hookean hyperelastic law:

$$\rho \frac{\partial^2 \boldsymbol{u}}{\partial t^2} \;=\; \boldsymbol{\nabla \cdot \sigma} \;+\; \rho \boldsymbol{g} \tag{3}$$

where,

$$\boldsymbol{\sigma} \;=\; \frac{1}{J}\left[\frac{K}{2}(J^2 \;-1)\boldsymbol{I} \;+\; \mu\, J^{-\frac{2}{3}} dev[\boldsymbol{F \cdot F^{\mathbf{T}}}]\right]$$

$$\boldsymbol{F} \;=\; \boldsymbol{I} \;+\; \boldsymbol{(\nabla_0 u)^{\mathbf{T}}}$$

$$\boldsymbol{J} = det[\boldsymbol{F}]$$

u = displacement vector
σ = stress

2.2.3 Fluid-Solid Interface

Kinematic and dynamic conditions hold at the interface between the fluid and solid regions.

The kinematic conditions state that the velocity and displacement must be continuous across the interface:

$$\mathbf{v}_{\mathbf{fluid}}^{[\mathbf{i}]} = \mathbf{v}_{\mathbf{solid}}^{[\mathbf{i}]} \tag{4}$$

$$\boldsymbol{u}_{\mathbf{fluid}}^{[\mathbf{i}]} = \mathbf{u}_{\mathbf{solid}}^{[\mathbf{i}]} \tag{5}$$

The dynamic conditions follow from linear momentum conservation and state that the forces are in equilibrium:

$$\boldsymbol{n}^{[\mathbf{i}]} \cdot \sigma_{\mathbf{fluid}}^{[\mathbf{i}]} = \mathbf{n}^{[\mathbf{i}]} \cdot \sigma_{\mathbf{solid}}^{[\mathbf{i}]} \tag{6}$$

2.3 Geometry and Mesh

The Geometry consists of a horizontal channel of 4 m in height and 8 m in length. A flexible flap of 0.1 m in width and 1 m in height is attached at the bottom of the channel at 2 m from the inlet. The aspect ratio of the flap is 10. The geometry is shown in the Figure 1.

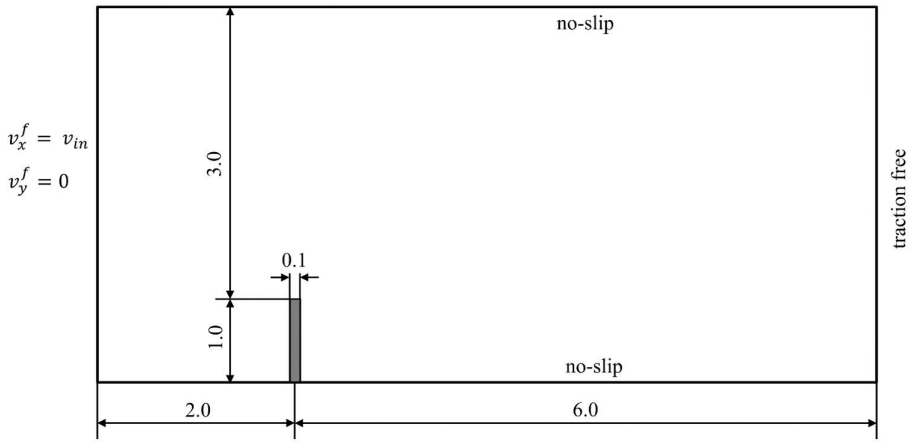

Figure 1: Computational domain and solid geometry

Meshing is done using OpenFoam BlockMesh Utility. In the FSI problem, while using the partitioned approach, the fluid domain and solid should be meshed separately since they are solved using different equations. The fluid domain is divided into six different blocks and simple grading

is used to create finer mesh near the solid as shown in Figure 2. Similarly, a solid domain is meshed considering it as a single block as shown in Figure 3. Only hexahedral cells are used during the meshing of both fluid and solid domains.

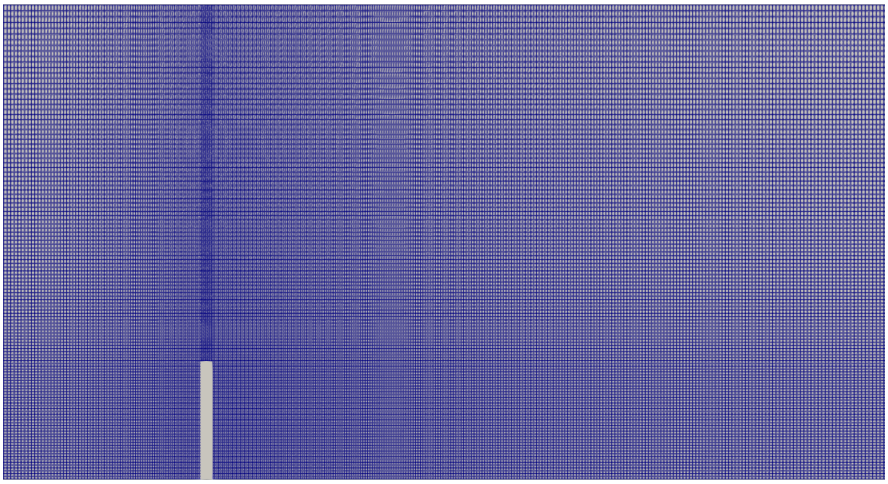

Figure 2: Mesh showing Fluid Domain

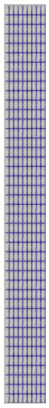

Figure 3: Mesh showing Solid

2.4 Solver setup

The solver setup can be breakdown into three different parts: Fluid Setup, Solid Setup, and Coupling Setup

2.4.1 Fluid Setup

2.4.1.1 Initial and Boundary Conditions

The velocity of the fluid at the inlet varies parabolically with the width of the flap as given by the equation 7. The mean velocity(v_m) at the inlet is 1 m/s. The velocity of the fluid in the y and z direction is kept at zero. The Reynolds number based on the velocity scale of v_m and length scale of the flap length ie. 1 m is considered to be 25.

$$v^f(0,\ y)\ =\ 6v_m\frac{y}{4.0}\left(1.0-\frac{y}{4.0}\right)\ m/s \tag{7}$$

The Boundary Conditions applied at all patches are given in the Table 1 and 2:

Patch	Velocity	Pressure
inlet	transitionalParabolicVelocity	zeroGradient
outlet	zeroGradient	fixedValue
flap	movingWallVelocity	zeroGradient
UpperWall	noSlip	zeroGradient
LowerWall	noSlip	zeroGradient
frontAndBack	empty	empty

Table 1: Boundary Conditions for fluid domain

Patch	Point Displacement
flap	solidTraction
bottom	fixedDisplacement
frontAndBack	empty

Table 2: Boundary Conditions for solid domain

2.4.1.2 Fluid Properties

The density of the fluid is considered to be 1 kg/m^3. Based on the Reynolds number value i.e. 25, the kinematic viscosity of the fluid is calculated using the equation 8.

$$Re\ =\ \frac{v_m l}{\nu} \tag{8}$$

The value of kinematic viscosity is obtained to be 4e-2 m^2/s using the length scale to be 1 m and mean velocity to be 1 m/s. The flow is assumed to be in the laminar regime.

2.4.1.3 Dynamic Mesh Treatment

A mesh morphing approach is used in Solids4Foam to update the mesh regularly as the solid deflects and changes the fluid mesh. VelocityLaplacian Solver is used to handle the mesh motion within which the diffusivity quadratic inverseDistance method is selected.

2.4.1.4 Finite Volume Schemes

Operation and their Schemes are tabulated in Table 3.

Operation	Scheme
Time Derivative	Backward
Gradient	Gauss Linear

Divergence	default none;
	div(phi,U) Gauss upwind;
	div((nuEff*dev2(T(grad(U))))) Gauss linear;
	div((nuEff*dev(T(grad(U))))) Gauss linear;

Laplacian	Gauss linear corrected
Surface Normal Gradient	corrected
Interpolation	linear

Table 3: Finite Volume Schemes

2.4.1.5 Solution Method and Control

A preconditioned Conjugate Gradient (PCG) solver is used for pressure with a Diagonal-based Incomplete Cholesky (DIC) preconditioner. smoothSolver with symGaussSeidal smoother is used to solve velocity and cell displacement. The tolerance for the pressure is used as 1e-8 and for velocity and cell displacement as 1e-6.

2.4.2 Solid Setup

2.4.2.1 Boundary Conditions

One end of the flap is attached rigidly to the bottom of the channel and the other end is set free to deflection. It acts like a cantilever beam. The flap is not allowed to deflect in the z direction. When the fluid imparts pressure and viscous force to the flap then the flap deflects and becomes steady when the flow becomes fully developed after some time.

2.4.2.2 Material Properties

The density ratio of solid and fluid is considered to be 10. The material properties of the flap i.e. solid are listed below:

- Density = 10 kg/m^3

- Young's Modulus = 20 KPa
- Poisson's Ratio = 0.3

2.4.2.3 Control

The time step of 1e−3 s is used.

2.4.3 Coupling Setup

Within the partitioned approach of two-way FSI, there can be two further different approaches: weak coupling and strong coupling. Weak coupling is also known as explicit coupling, and strong coupling is also known as implicit coupling. In implicit coupling, multiple iterations are done within a single coupling timestep to satisfy the dynamic and kinematic coupling conditions. In explicit coupling, only a single iteration is done without regard for dynamic and kinematic coupling conditions. In FSI cases like this, where the deflection is large, implicit coupling is a better approach as the accumulated error becomes too significant in explicit coupling. Two different coupling algorithms are used namely AITKEN and IQNILS. The tolerance for the FSI loop within each time-step is used as 1e-6 and similarly maximum number of outer FSI loop correctors within each time-step is kept as 20. The relaxation factor is kept to 0.1 and the coupling is enabled from the start. DirectMap is used as the method for transferring information between the interfaces.

3 Results and Discussions

3.1 Convergence Tests

3.1.1 Grid Size Convergence Test

Three different meshes are made using blockMesh for the Grid Convergence Test. It is done to ensure the results are independent of the cell size. A mesh refinement factor of two is used to create the coarse, medium, and fine mesh. This is done for the solid and fluid domains separately. The number of cells for all three coarse, medium, and fine mesh is tabulated in the Table 4 for fluid and solid separately.

Mesh	Fluid Domain	Solid
Fine	42997	378
Medium	21625	180
Coarse	10815	84

Table 4: Number of cells for different meshes

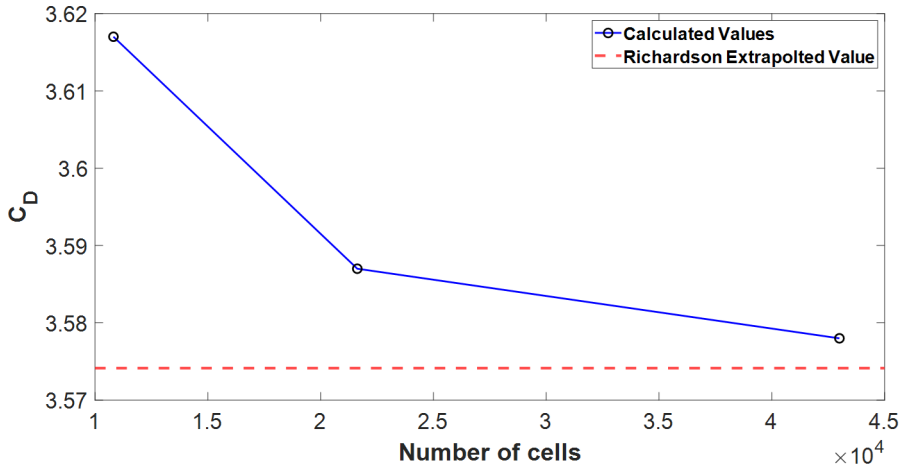

Figure 4: Grid Convergence Study

The dimensionless displacement and the drag coefficient for three different meshes are tabulated in the Table 5 and 6 using both AITKEN and IQNILS coupling algorithms. Richardson extrapolation is done using the methodology mentioned in reference [5] to obtain the drag coefficient values when the cell size tends to zero. Ideally, this means an infinite number of cells in the fluid and solid domain.

AITKEN	Displacement	Drag Coefficient (C_D)
Coarse	0.1183	3.617
Medium	0.1236	3.587
Fine	0.1264	3.578

Table 5: Values obtained using AITKEN coupling algorithm

IQNILS	Displacement	Drag Coefficient (C_D)
Coarse	0.1184	3.616
Medium	0.1244	3.603
Fine	0.1272	3.596

Table 6: Values obtained using IQNILS coupling algorithm

Then the relative percentage error is calculated for the drag coefficient values obtained for all three meshes by comparing with the Richardson extrapolated value i.e. 3.5741 for C_D which is shown in Table 7. By setting the criteria to be 0.4 % error and computational time, the medium mesh is chosen as the best one.

Mesh	Drag Coefficient (C_D)	Relative Error (%)
Coarse	3.617	1.2
Medium	3.587	0.36
Fine	3.578	0.10

Table 7: Comparison with richardson extrapolated value

3.1.2 Time Step Convergence Test

Time step convergence study is not done due to limited computational resources.

3.2 Validation

The converged values of drag coefficient and displacement for both the AITKEN and IQNILS coupling algorithms are compared with each other. Similarly, the data obtained with solids4foam is again compared with the results obtained with different solvers. The values are within the relative error of 3 % for both AITKEN and IQNILS.

3.3 Results

The x direction displacement is normalized with the length scale of the flap and similarly, time is normalized using mean inlet velocity and length scale. The mean inlet velocity in our case is 1 m/s and the length scale is 1m. This is done for the ease of comparing data with the flap having different lengths. Dimensionless displacement versus dimensionless time is plotted and compared with the results obtained from other solvers as shown in Figure 5. Similarly, the drag coefficient is plotted against normalized time and compared with the results obtained from other solvers as shown in Figure 6.

In Figure 8, displacement contours for the flexible flap and velocity contours in the fluid domain are shown simultaneously. It shows the position of the flap when the flap attains steady deflection after the flow becomes fully developed.

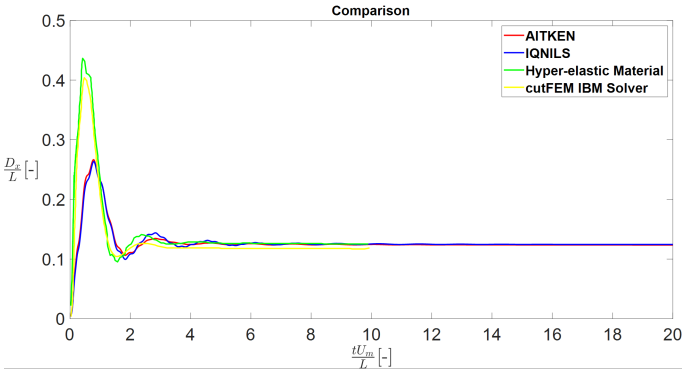

Figure 5: Displacement Comparison using different solvers

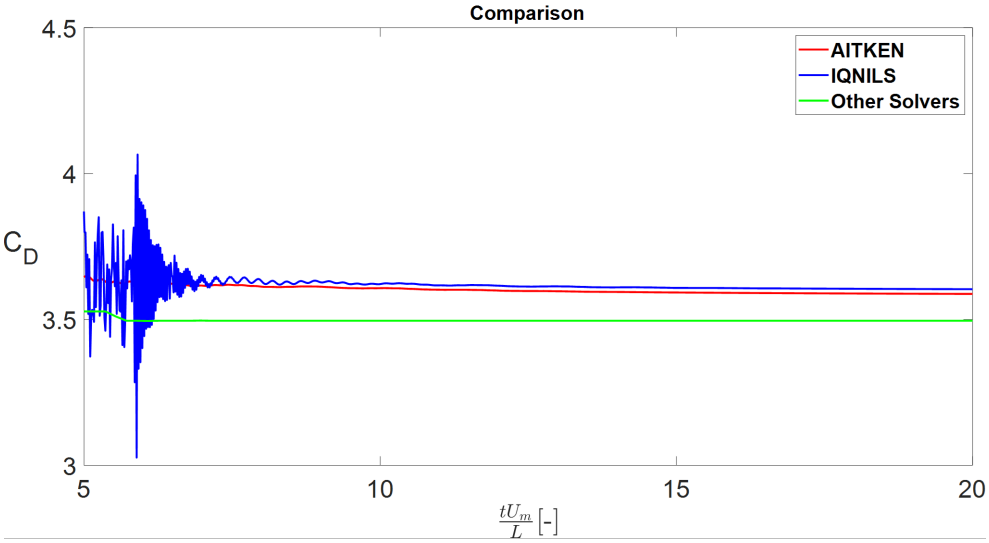

Figure 6: Drag Coefficient Comparison using different solvers

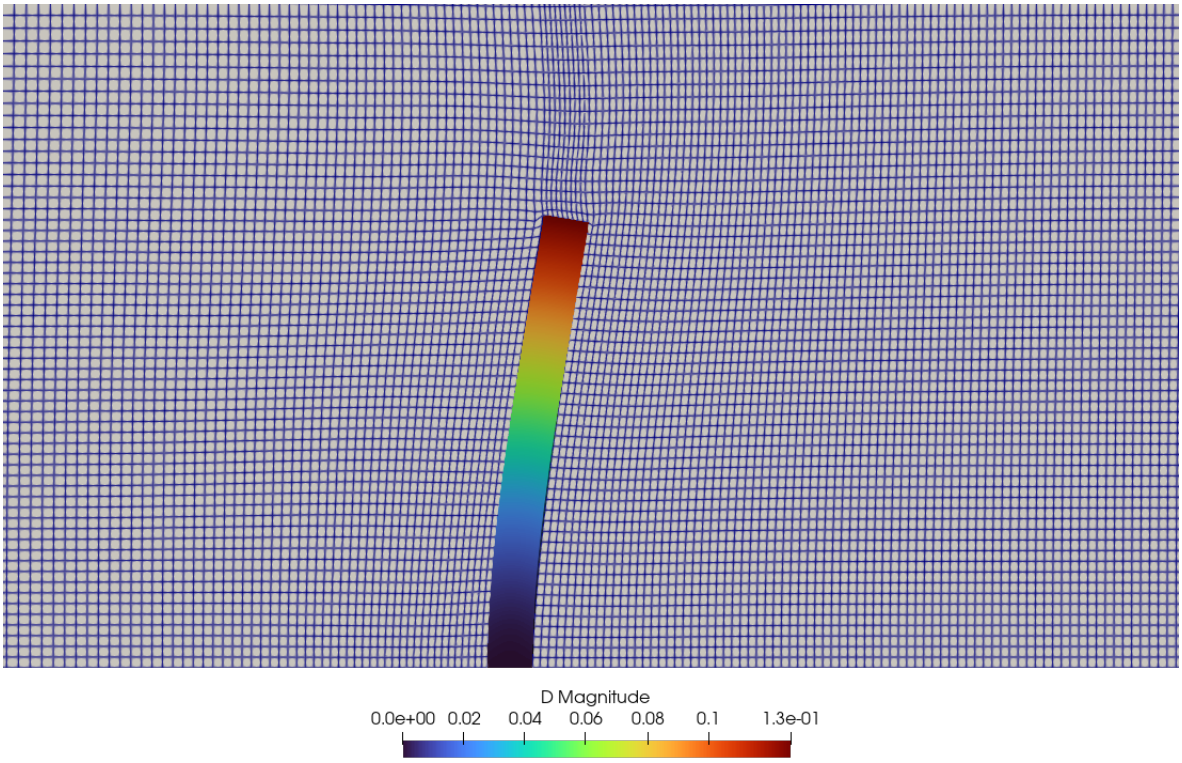

Figure 7: Mesh Morphing

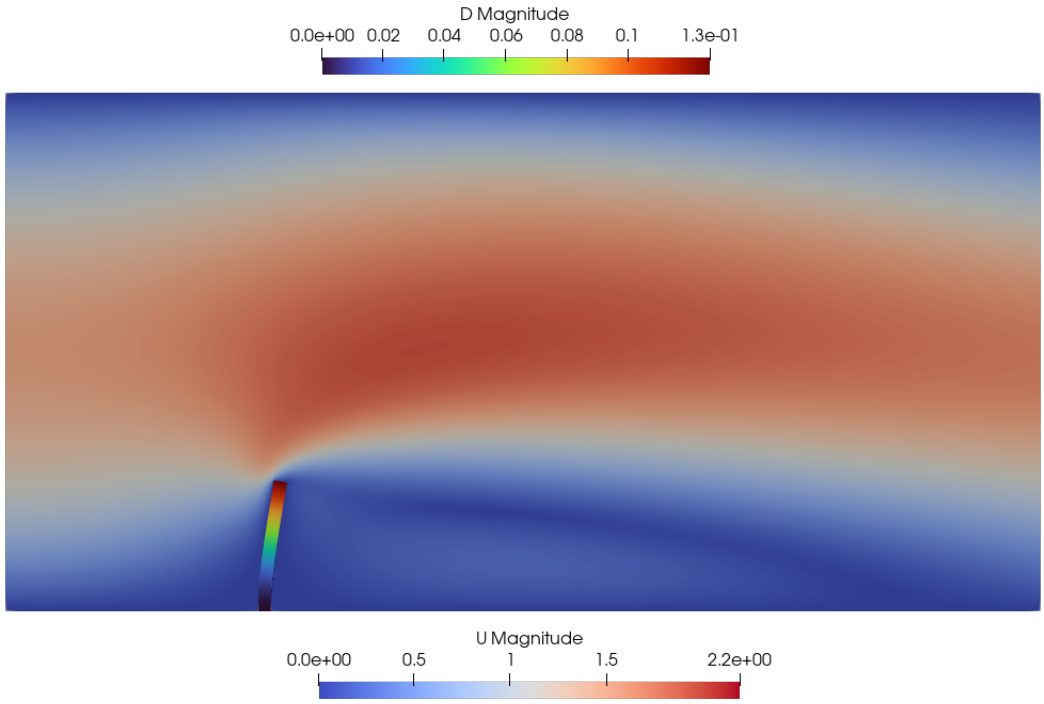

Figure 8: Displacement and Velocity Contours

4 Conclusions

In this study, the FSI between the flexible perpendicular flap and laminar incompressible flow has been done using the solids4foam solver. The density ratio between solid and fluid has been used as 10 with the flow Reynolds number being 25. The FSI has been done using two different coupling algorithms i.e. AITKEN and IQNILS and compared with each other as well as with the results obtained from the other solvers. To get the steady values of drag coefficient and displacement, tolerance for the FSI loop within each time-step has been kept as 1e-6. The tolerance values higher than 1e-6 result in the oscillation in the values of drag coefficient and displacement.

CASE 2: HronTurek Case

5 Governing Equations and Models

5.1 Problem definition

This study investigates the FSI between elastic plate and laminar incompressible flow. The geometry of the problem consists of a rectangular horizontal channel and a rigid cylinder. An elastic bar is attached to the right hand side of the rigid cylinder. The problem is based on the well known CFD

benchmark in [4] popularly known as HronTurek Case. This FSI problem results in the self induced oscillations of the structure i.e. elastic bar.

5.2 Governing equations

Fluid, solid, and the interface between them are governed by three sets of equations.

5.2.1 Fluid

The fluid is considered to be Newtonian, incompressible and its state is described by the velocity and pressure fields i.e. v^f and p^f. The balance equations are:

$$\rho^f \frac{\partial v^f}{\partial t} + \rho^f \left(\nabla v^f\right) v^f = div\ \sigma^f \tag{9}$$

$$div\ \boldsymbol{v}^{\mathbf{f}} = 0 \tag{10}$$

The material constitutive equation is

$$\boldsymbol{\sigma}^{\mathbf{f}} = -p^f \boldsymbol{I} + \rho^f \nu^f \left(\nabla \boldsymbol{v}^{\mathbf{f}} + \nabla \boldsymbol{v}^{\mathbf{f}\ T}\right) \tag{11}$$

5.2.2 Solid

The structure is assumed to be elastic and compressible. Its configuration is described by the displacement u^s, with velocity field $v^s = \frac{\partial u^s}{\partial t}$. The balance equations are:

$$\rho^s \frac{\partial^2 \boldsymbol{v}^{\mathbf{s}}}{\partial t^2} + \rho^s \left(\nabla \boldsymbol{v}^{\mathbf{s}}\right) \boldsymbol{v}^{\mathbf{s}} = div\left(\boldsymbol{\sigma}^{\mathbf{s}}\right) + \rho^s \boldsymbol{g} \tag{12}$$

The material is specified by giving the Cauchy stress tensor (σ^s) by the following constitutive law for the St. Venant-Kirchhoff material

$$\boldsymbol{E} = \frac{1}{2}\left(\boldsymbol{F}^{\mathbf{T}}\boldsymbol{F} - \boldsymbol{I}\right) \tag{13}$$

$$\boldsymbol{\sigma}^{\mathbf{s}} = \frac{1}{J}\boldsymbol{F}\left(\lambda^s\left(tr\ \boldsymbol{E}\right)\boldsymbol{I} + 2\mu^s \boldsymbol{E}\right)\ \boldsymbol{F}^T \tag{14}$$

5.2.3 Fluid-Solid Interface

The boundary conditions on the fluid solid interface are assumed to be

$$\mathbf{v}_{\mathbf{f}}^{[\mathbf{i}]} = \mathbf{v}_{\mathbf{s}}^{[\mathbf{i}]} \tag{15}$$

$$\boldsymbol{u}_{\mathbf{fluid}}^{[\mathbf{i}]} = \mathbf{u}_{\mathbf{solid}}^{[\mathbf{i}]} \tag{16}$$

$$\boldsymbol{n}^{[\mathbf{i}]} \cdot \sigma_{\mathbf{fluid}}^{[\mathbf{i}]} = \mathbf{n}^{[\mathbf{i}]} \cdot \sigma_{\mathbf{solid}}^{\ [\mathbf{i}]} \tag{17}$$

where n is a unit normal vector to the fluid solid interface. This implies the no-slip condition for the flow, and that the forces on the interface are in balance.

5.3 Geometry and Mesh

The Geometry consists of a horizontal channel of 0.41 m in height and 2.5 m in length. A flexible flap of 0.02 m in width and 0.35 m in length is attached at the right hand side of the rigid cylinder of radius 0.05 m. The center of cylinder C is at (0.2, 0.2) m measured from the left bottom of the channel which is considered to be at origin. The control points are A(t), fixed with the structure with A(0) = (0.6, 0.2) m, and B = (0.15, 0.2) m where B is the leading edge of the rigid cylinder to the flow. The setting is intentionally unsymmetric to prevent the dependence of the onset of any possible oscillation on the precision of the computation. The geometry is shown in the Figure 9.

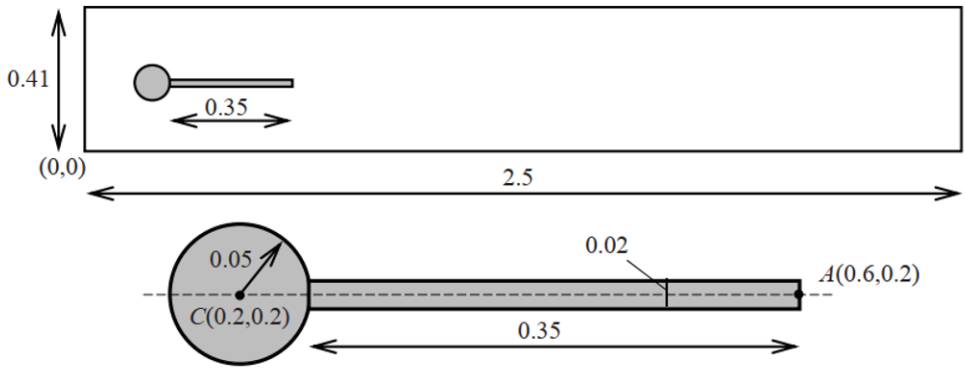

Figure 9: Computational Domain showing HronTurek Case

Meshing is done using Gmesh, an opensource meshing tool. In the FSI problem, while using the partitioned approach, the fluid domain and solid should be meshed separately since they are solved using different equations. The fluid domain is divided into eighteen different blocks and simple grading is used to create structured mesh near the rigid cylinder and elastic bar as shown in Figure 10. Similarly, a solid domain is meshed considering it as a single block as shown in Figure 11. Only hexahedral cells are used during the meshing of both fluid and solid domains.

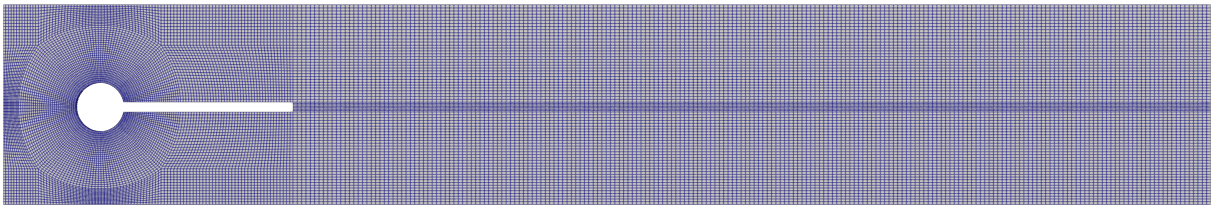

Figure 10: Mesh showing Fluid Domain

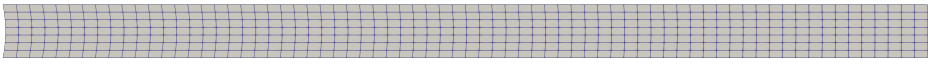

Figure 11: Mesh showing Solid Domain

5.4 Solver setup

The solver setup can be breakdown into three different parts: Fluid Setup, Solid Setup, and Coupling Setup

5.4.1 Fluid Setup

5.4.1.1 Initial and Boundary Conditions

The velocity of the fluid at the inlet varies parabolically with the width of the flap as given by the equation 18. There are actually 3 variants of this problem FSI1, FSI2 and FSI3 where FSI1 has steady state solution and other two results in periodic solutions. Only FSI 2 and FSI3 is analyzed with reference to the benchmark paper.

$$v^f(0,\ y)\ = 1.5\ \overline{U}\frac{4.0}{0.1681}y\ (0.41 - y)\ \ m/s \tag{18}$$

The Boundary Conditions applied at all patches are given in the Table 8 and 9:

Patch	Velocity	Pressure
inlet	transitionalParabolicVelocity	zeroGradient
outlet	zeroGradient	fixedValue
plate	newMovingWallVelocity	zeroGradient
cylinder	fixedValue	zeroGradient
bottom	fixedValue	zeroGradient
top	fixedValue	zeroGradient
frontAndBack	empty	empty

Table 8: Boundary Conditions for fluid domain

Patch	Point Displacement
plate	solidTraction
plateFix	fixedDisplacement
frontAndBack	empty

Table 9: Boundary Conditions for solid domain

5.4.1.2 Fluid Properties

The density of the fluid is considered to be 1000 kg/m^3. The value of kinematic viscosity is used to be 1e-3 m^2/s for both FSI2 and FSI3. The mean inlet velocity is 1 m/s and 2 m/s for FSI2 and FSI3 respectively. The flow is assumed to be in the laminar regime.

5.4.1.3 Dynamic Mesh Treatment

A mesh morphing approach is used in Solids4Foam to update the mesh regularly as the solid deflects and changes the fluid mesh. VelocityLaplacian Solver is used to handle the mesh motion within which the diffusivity quadratic inverseDistance method is selected.

5.4.1.4 Finite Volume Schemes

Operation and their Schemes are tabulated in Table 10.

Operation	Scheme
Time Derivative	Backward
Gradient	leastSquares

Divergence	default none;
	div(phi,U) Gauss upwind;
	div((nuEff*dev2(T(grad(U))))) Gauss linear;
	div((nuEff*dev(T(grad(U))))) Gauss linear;

Laplacian	Gauss linear corrected
Surface Normal Gradient	corrected
Interpolation	linear

Table 10: Finite Volume Schemes

5.4.1.5 Solution Method and Control

A GAMG solver with GaussSeidel smoother is used for pressure and cell displacemwnt. PBiCG with a DILU preconditioner is used for the velocity. The tolerance for the pressure, velocity and cell displacement is used as 1e-6.

5.4.2 Solid Setup

5.4.2.1 Boundary Conditions

Left end of the elastic bar is attached rigidly to the right hand side of fixed cylinder and the other end is set free to deflection. It acts like a cantilever beam. The bar is not allowed to deflect in the z direction. When the fluid imparts pressure and viscous force to the bar then the bar deflects and starts oscillating when the flow becomes fully developed after two seconds.

5.4.2.2 Material Properties

The density of elastic bar is 10,000 kg/m3 and 1000 kg/m3 for FSI2 and FSI3 case respectively. The material properties of the elastic bar i.e. solid for both FSI2 and FSI3 are tabulated below in Table 11.

Properties	FSI2	FSI3
Density (kg/m^3)	10,000	1000
Young's Modulus (MPa)	1.4	5.6
Poisson's ratio	0.4	0.4

Table 11: Solid Properties for FSI2 and FSI3

5.4.2.3 Control

The time step of 1e−3 s is used.

5.4.3 Coupling Setup

Within the partitioned approach of two-way FSI, there can be two further different approaches: weak coupling and strong coupling. Weak coupling is also known as explicit coupling, and strong coupling is also known as implicit coupling. In implicit coupling, multiple iterations are done within a single coupling timestep to satisfy the dynamic and kinematic coupling conditions. In explicit coupling, only a single iteration is done without regard for dynamic and kinematic coupling conditions. In FSI cases like this, where the deflection is large, implicit coupling is a better approach as the accumulated error becomes too significant in explicit coupling. IQNILS is used as the coupling algorithm for the fluid solid interface. The tolerance for the FSI loop within each time-step is used as 1e-6 and similarly maximum number of outer FSI loop correctors within each time-step is kept as 30. The relaxation factor is kept to 0.05 and the coupling is enabled after two second when the flow becomes fully developed.

6 Results and Discussions

6.1 Convergence Tests

6.1.1 Grid Size Convergence Test

Three different meshes are made using Gmesh for the Grid Convergence Test. It is done to ensure the results are independent of the cell size. A mesh refinement factor of two is used to create the coarse, medium, and fine mesh. This is done for the solid and fluid domains separately. The number of cells for all three coarse, medium, and fine mesh is tabulated in the Table 12 for fluid and solid separately.

Richardson extrapolation is done using the methodology mentioned in reference [5] to obtain the drag force when the cell size tends to zero. Ideally, this means an infinite number of cells in the fluid and solid domain. Then the relative percentage error is calculated for the drag coefficient values obtained for all three meshes by comparing with the Richardson extrapolated value which is shown in Table 13. By setting the criteria to be 1.5 % error and computational time, the medium mesh is chosen as the best one.

Mesh	Fluid Domain	Solid
Fine	12063	205
Medium	5787	102
Coarse	2788	48

Table 12: Number of cells for different meshes

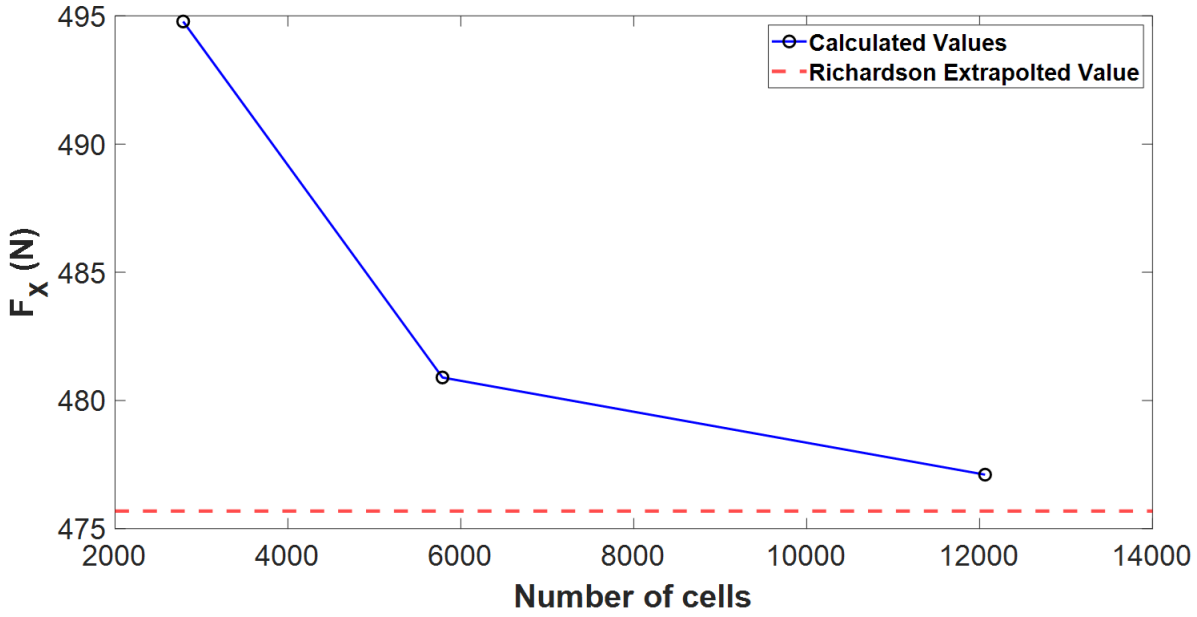

Figure 12: Grid Convergence Study considering F_x

Mesh	Force (F_x)	Relative Error (%)
Coarse	494.782	4.01
Medium	480.897	1.09
Fine	477.107	0.29

Table 13: Comparison with richardson extrapolated value

6.2 Validation

The converged values of forces and displacement in x and y direction for both FSI2 and FSI3 case are compared with benchmark values as tabulated in Table 14 and 15. The format of the data is mean ± amplitude[frequency].

FSI2	Benchmark	solids4Foam
$F_x(N)$	208.83 ± 73.75[3.8]	231.8215 ± 111.2485[4.44]
$F_y(N)$	0.88 ± 234.2[2.0]	1.1815 ± 352.2195[2.2676]
$D_x(mm)$	−14.58 ± 12.44[3.8]	-16.3165 ± 15.2522[4.44]
$D_y(mm)$	1.23 ± 80.6[2.0]	0.8832 ± 78.9590[2.2676]

Table 14: Comparison of FSI2 data with Benchmark

FSI3	Benchmark	solids4Foam
$F_x(N)$	457.3 ± 22.66[10.9]	480.897 ± 36.625[12.1951]
$F_y(N)$	2.22 ± 149.78[5.3]	0.999 ± 403.434[6.0241]
$D_x(mm)$	−2.69 ± 2.53[10.9]	-1.5903 ± 1.4607[12.1951]
$D_y(mm)$	1.48 ± 34.38[5.3]	1.7562 ± 25.0993[6.0241]

Table 15: Comparison of FSI3 data with Benchmark

6.3 Results

Mean values and amplitudes are calculated using the maximum and the minimum values after the periodic solution has been reached (around 4 s for the FSI3 case), where frequencies are calculated using the Fast Fourier Transform algorithm. The difference between the calculated and the benchmark results is around 5% in average for the amplitude and frequency of force and displacement. The relative difference for the mean value of the force y-component goes up to 40%, which can be attributed to the difficulty in calculating the mean value in the case when it is close to zero as mentioned in [1]. X and Y displacement are plotted against time as shown in Figure 13 and 14. Similarly, the lift and drag forces are plotted against time as shown in Figure 15.

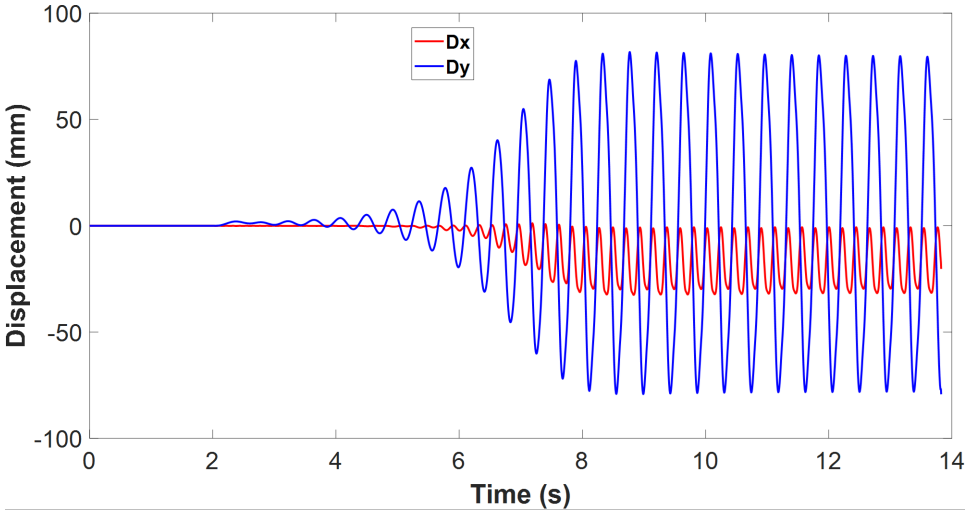

Figure 13: Displacement plot for FSI2

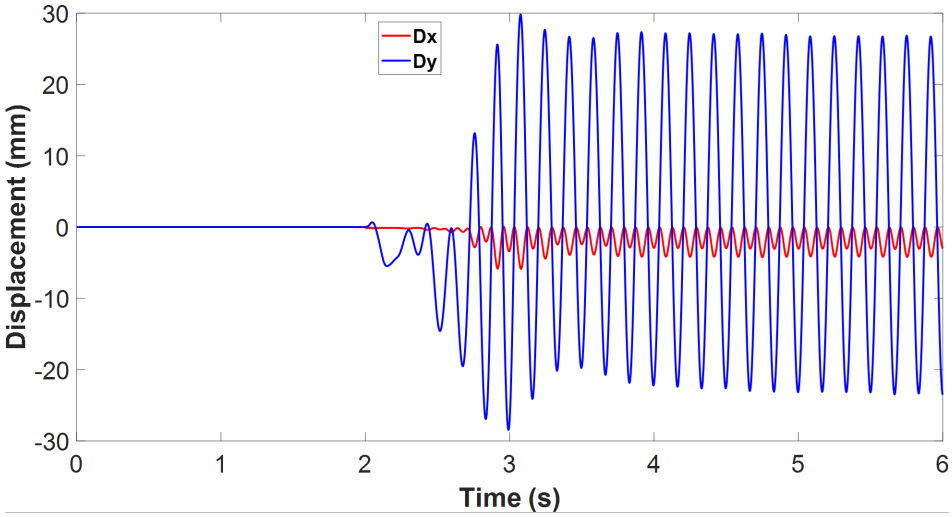

Figure 14: Displacement plot for FSI3

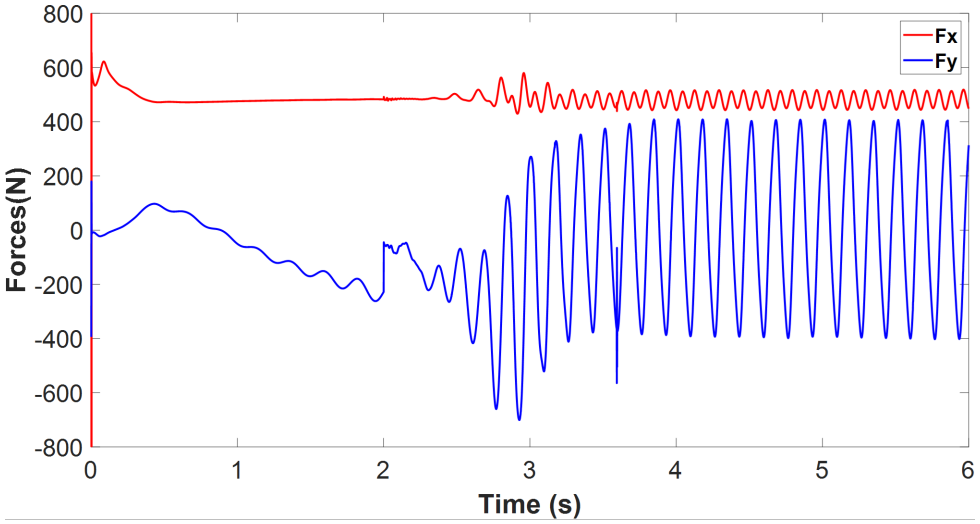

Figure 15: Force plot for FSI3

In Figure 17, displacement contours for the elastic bar and velocity contours in the fluid domain are shown simultaneously. It shows the position of the bar when the bar is oscillating after the flow becomes fully developed. Similarly, mesh motion of fluid domain due to elastic bar deflection is shown in Figure 16.

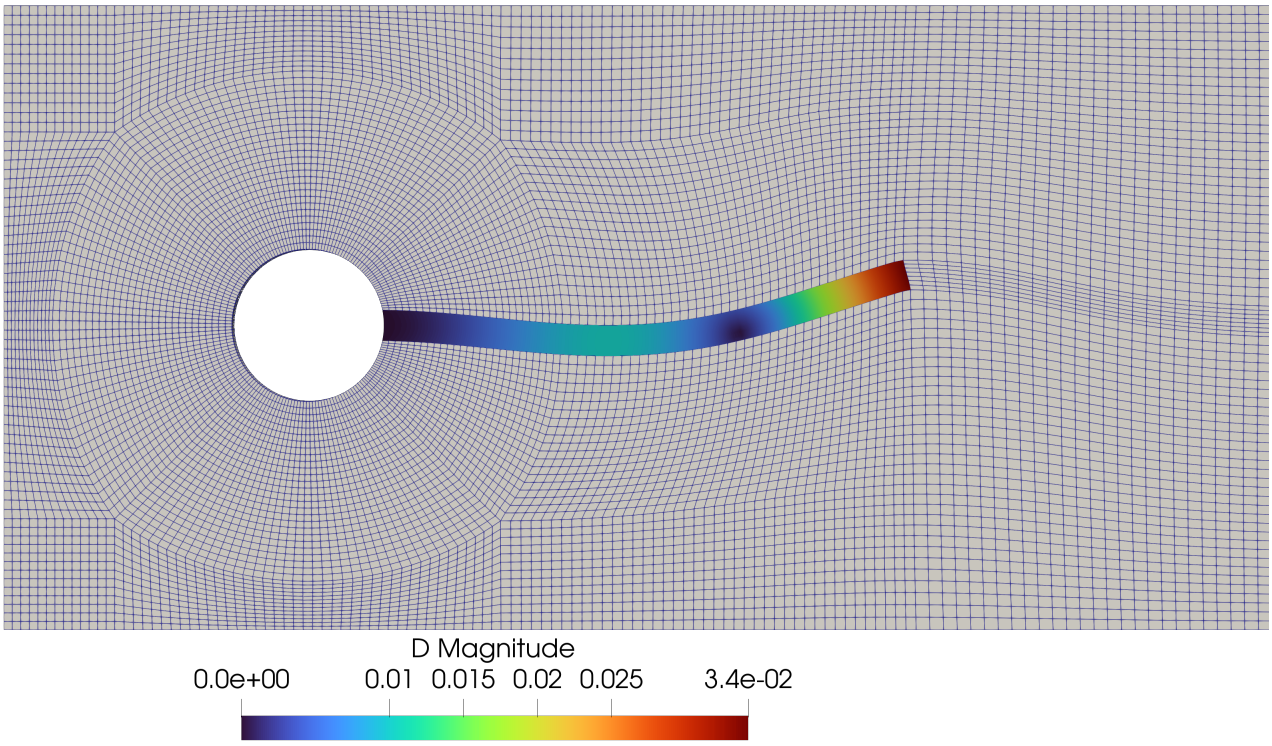

Figure 16: Mesh Motion due to bar oscillation

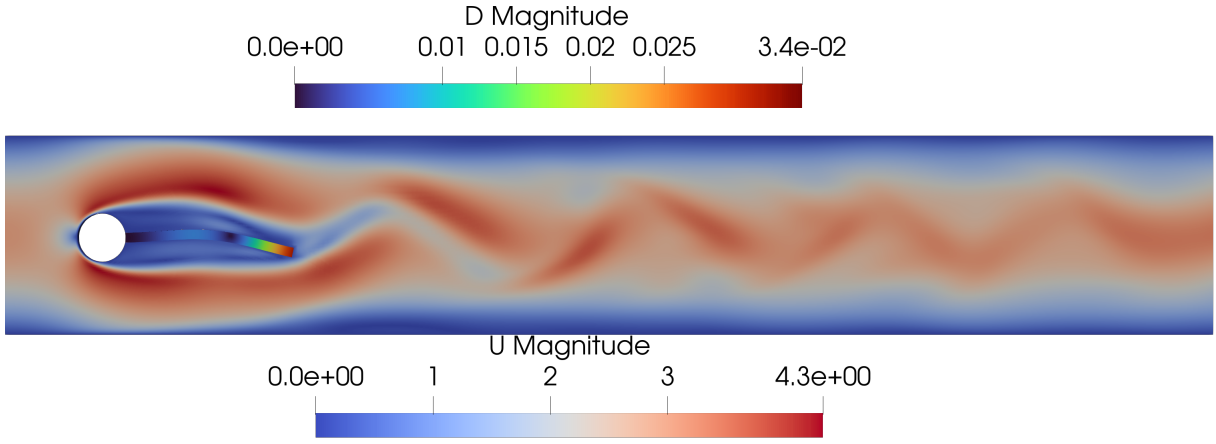

Figure 17: Contours when elastic bar is in deflected position

7 Conclusions

In this study, the FSI between the flexible elastic bar and laminar incompressible flow has been done using the solids4foam solver taking reference as the benchmark paper. Two different cases of HronTurek Problem are analyzed i.e. FSI2 and FSI3 cases with different properties of solid and

fluid. To get the steady values of drag force and displacement, simulation is run for 6 sec and 10 sec for FSI2 and FSI3 case respectively.

8 Acknowledgement

First and foremost, I'd want to express my profound appreciation to Dr. Chandan Bose, my supervisor, whose excellent insights and direction from the project's creation to completion were critical to its success and provided me with an invaluable learning experience. This endeavor would not have been feasible without him. I'd also want to thank Mr. Harish Jayaraj, my mentor for his important technical assistance. Last but not least, I'd like to thank Mrs. Payel Mukherjee, the FOSSEE team, and IIT Bombay for giving the opportunity, resources, and support necessary for the project's success.

References

[1] P. Cardiff, "solids4foam," 2020, accessed on 4-30-2024. [Online]. Available: http://www.solids4foam.com

[2] Philip Cardiff, "Training: Solid mechanics and fluid-solid interaction using the solids4foam toolbox," 06 2020.

[3] Z. Tuković, A. Karač, P. Cardiff, H. Jasak, and A. Ivanković, "Openfoam finite volume solver for fluid-solid interaction," *Transactions of FAMENA*, vol. 42, no. 3, pp. 1–31, 2018. [Online]. Available: https://hrcak.srce.hr/206941

[4] S. Turek and J. Hron, "Proposal for numerical benchmarking of fluid-structure interaction between an elastic object and laminar incompressible flow," in *Fluid-Structure Interaction*, H.-J. Bungartz and M. Schäfer, Eds. Berlin, Heidelberg: Springer Berlin Heidelberg, 2006, pp. 371–385.

[5] P. J. Roache, "QUANTIFICATION OF UNCERTAINTY IN COMPUTATIONAL FLUID DYNAMICS," *Annual Review of Fluid Mechanics*, vol. 29, no. 1, pp. 123–160, Jan. 1997. [Online]. Available: https://www.annualreviews.org/doi/10.1146/annurev.fluid.29.1.123